Development of Planning-Stage Models for Analyzing Continuous Flow Intersections

Xianfeng Yang[1]; Gang-Len Chang, M.ASCE[2]; Saed Rahwanji[3]; and Yang Lu, Ph.D.[4]

Abstract: Despite the increasing use of continuous-flow intersections (CFIs) to contend with the congestion caused by heavy through and left-turn traffic flows, a reliable and convenient tool for the traffic community to identify potential deficiencies of a CFI's design is not yet available. This is due to the unique geometric feature of CFI, which comprises one primary intersection and several crossover intersections. The interdependent relationship between traffic delays and queues at a CFI with five closely spaced intersections cannot be fully captured with the existing analysis models, which were developed primarily for conventional intersections. In response to such a need, this study presents a comprehensive analysis for the overall CFI delay, identifies the potential queue spillback locations, and develops a set of planning-stage models for the CFI design geometry. To facilitate the application of these proposed models, this paper also includes a case study of a CFI at the intersection of MD 4 and MD 235 constructed by the Maryland State Highway Administration. **DOI: [10.1061/(ASCE)TE.1943-5436 .0000596](#).** *© 2013 American Society of Civil Engineers.*

CE Database subject headings: Intersections; Geometry; Traffic engineering.

Author keywords: Continuous-flow intersection; Geometric features; Planning model; Link length design.

Introduction

The continuous-flow intersection (CFI) has attracted increasing attention during recent years. The main benefit of a CFI is the elimination of the conflict between left-turn and opposing through traffic by relocating the left-turn bay a significant distance upstream of the primary intersection so that the through and left-turn flows can move concurrently. With the presence of left-turn crossovers, a full CFI design, with its primary and crossover intersections, generally leads to a larger footprint than a typical conventional intersection. For a full CFI design, the primary intersection is located at the center, where four crossover intersections, also known as "left crossovers," are placed respectively on four approaching legs. Such a design allows all intersections in the CFI to operate with a two-phase signal.

Due to the increasing applications of CFI over recent years, some fundamental issues associated with its operational efficiency and capacity have emerged as priority research subjects of the traffic community. For example, Goldblatt et al. ([1994](#)) showed that the benefits of CFIs are particularly pronounced when the volumes to some approaches exceed the capacity of a conventional intersection. Using simulation data from CORSIM, Hummer ([1998a, b](#)) and Reid ([1999, 2001](#)) compared the performance of seven different unconventional designs with a conventional intersection under heavy left-turn volumes and indicated that the CFI has great potential to accommodate the heavy demand that has a high percentage of left-turn volume. Jagannathan ([2004](#)) carried out a series of studies on the delays that occur at CFIs based on both the simulation and regression results.

In a later study, Cheong et al. ([2008](#)) compared the performances of several CFIs under balanced and unbalanced volume conditions and reported that switching a conventional intersection to CFI can reduce the total delay approximately by 60–85%. Kim et al. ([2007](#)) applied their concepts to selected locations for CFI design. El Esawey and Sayed ([2007](#)) reported similar results and further argued that the capacity improvement of a CFI design is insensitive to an increase in the left-turn volume ratio. A field study by Pitaksringkarn ([2005](#)) also confirmed that a CFI design can reduce the intersection delays and queues by 64 and 61%, respectively, during peak hours. A report published by the Federal Highway Administration ([Hughes et al. 2010](#)) offers a comprehensive review of the geometric features, safety performance, operational efficiency, and construction cost of different CFI designs.

In summary, existing studies, such as El Esawey and Sayed ([2007](#)), Hildebrand ([2007](#)), and Inman ([2009](#)), have consistently concluded that CFI outperforms conventional intersection, especially under the high traffic demand and high left-turn volume scenarios. Nevertheless, many critical issues associated with CFIs remain to be investigated. For instance, although many studies reported significant reductions in delays, the critical contributing factors and their respective impacts on such performance improvement is not yet well identified. The correlation between intersection delay and key geometric features, such as bay length, was not studied. In fact, a CFI can be viewed as a small network comprising five intersection nodes and several interconnected links. Hence, the delays associated with different traffic movements are affected not only by the volume-to-capacity ratio at each intersection, but also

[1]Ph.D. Candidate, Dept. of Civil and Environmental Engineering, Univ. of Maryland, 1173 Glenn L. Martin Hall, College Park, MD 20742 (corresponding author). E-mail: xyang125@umd.edu

[2]Professor, Dept. of Civil and Environmental Engineering, Univ. of Maryland, 1173 Glenn L. Martin Hall, College Park, MD 20742. E-mail: gang@umd.edu

[3]Assistant Division Chief, Office of Traffic and Safety, Maryland State Highway Administration, 7491 Connelley Dr., Hanover, MD 21076. E-mail: srahwanji@sha.state.md.us

[4]Dept. of Civil and Environmental Engineering, Univ. of Maryland, 1173 Glenn L. Martin Hall, College Park, MD 20742. E-mail: yanglu83@umd.edu

by the queue lengths along all associated links. Although El Esawey and Sayed (2007) pointed out that the improved capacity by CFI may be related to its unique geometric layout, no subsequent research is available along this direction.

The rest of this paper is organized as follows: the "Performance Analysis" section introduces the data set for simulation experiments and performs the delay analysis for a full CFI design. "Queue Length Estimation" presents a set of regression models for the queue length estimation. "Model Application Process" discusses the proposed planning and evaluation process, and "Case Study" studies a real-world case. The final section summarizes the conclusions and ongoing research.

Performance Analysis

Despite the fact that existing studies have generally concluded the superior performance of CFIs over conventional intersections, identification of critical contributing factors remains an ongoing research issue. This paper presents preliminary investigation results on this subject using field data along with simulation analysis. The primary purpose is to produce a set of statistical models for evaluation of a CFI design under various projected traffic demands at its planning stage.

Experimental Design

Recognizing that a simulation system is useful only if it can faithfully reflect the behaviors of its target driving populations, the simulation calibration is an essential step in this study. A typical calibration procedure includes (1) data collection, (2) selection of the calibration objective function, (3) selection of key parameters to be calibrated, and (4) searching for the optimal values of those parameters.

This study has conducted a field study at a CFI intersection (the intersection of MD 210 and MD 228 in Maryland). The calibration of simulation parameters is performed by minimizing the following objective function:

$$\min \frac{1}{N} \sum_{i=1}^{N} (Q_{bi} - Q_{si})^2 \tag{1}$$

where Q_{bi} = observed maximum queue length at cycle i; Q_{si} = simulated maximum queue length at cycle i; and N = number of cycles observed.

The simulator calibration was conducted with a standard genetic algorithm (GA). Table 1 summarizes the primary driving behavior parameters of *VISSIM* after calibration with the field data.

To generate the experimental data with the calibrated simulator, four scenarios with different geometric parameters are used to investigate impact on a CFI's performance. Table 2 summarizes the geometric parameters adopted in the simulation experiments.

Incoming traffic demands are generated from the most upstream end of those four CFI legs, where the simulation employs the Poisson process for traffic arrivals. A total of 600 volume sets are randomly generated for each scenario and simulated with *VISSIM*. To reduce the output variation due to the stochastic properties of microscopic simulation, each demand scenario has been simulated for 30 replications under different initial random seeds. The simulation duration for each case is set to be 2 h, and the traffic flow rates remain unchanged within this time frame.

Delay Analysis of CFI

Jagannathan (2004) derived the following delay model for CFI, assuming an exponential relation between average delay and traffic volumes:

$$d = \exp\left[a_0 + \left(\sum_{ij} a_{ij} X_{ij}\right) \Big/ 10^4\right] \tag{2}$$

where X_{ij} = flow rates from approach i and movement group j. However, the experimental data reveals that the average delay depends not only on traffic flow rates but also on the ratio between the maximum queue length and its corresponding link length at the intersection.

Fig. 1 plotted the average delay per vehicle against several potential contributing factors. Fig. 1(a) shows the relationship between the average delay and the total demand, revealing that both the mean value and the variance of delay increase linearly with the total intersection volume. Fig. 1(b) presents the relationship between average delay and the average critical lane volume of CFI. The critical lane volume (CLV) is an indicator of the total conflicting flows within an intersection. Because a full CFI consists of five subintersections, one can measure the congestion level of such a small signalized network with the arithmetic mean of CLV from each subintersection. Fig. 1(b) shows a clear exponential relation between the average delay and average CLV. The variance of the average delay also increases with CLV, where the distribution of delays becomes widely spread at the high volume range.

Fig. 1(c) illustrates the relationship between the average delay and queuing size within a CFI. The QL ratio is defined as the ratio between the maximum queue length and the available bay (or link) length, as shown in Eq. (3):

$$\text{QL ratio} = \frac{\text{Maximum queue length}}{\text{Bay length}} \tag{3}$$

If the QL ratio of a bay is less than 1, it indicates that the design can provide a sufficient storage capacity to accommodate all volumes approaching the target bay. In contrast, if it is greater than 1, queue spillback may incur at that link due to insufficient bay

Table 1. Driving Behavior Parameters of *VISSIM*

Parameters	Value
Maximum acceleration	2.99 m/s^2 (9.8 ft/s^2)
Desired acceleration	1.89 m/s^2 (6.2 ft/s^2)
Look-ahead distance	0 ∼ 250 m
Probability of temporary lack of attention	10%
Duration of temporary lack of attention	0.3 s
Average stand-still distance	2.32 m

Table 2. Geometric Parameters Used in Simulation Experiments

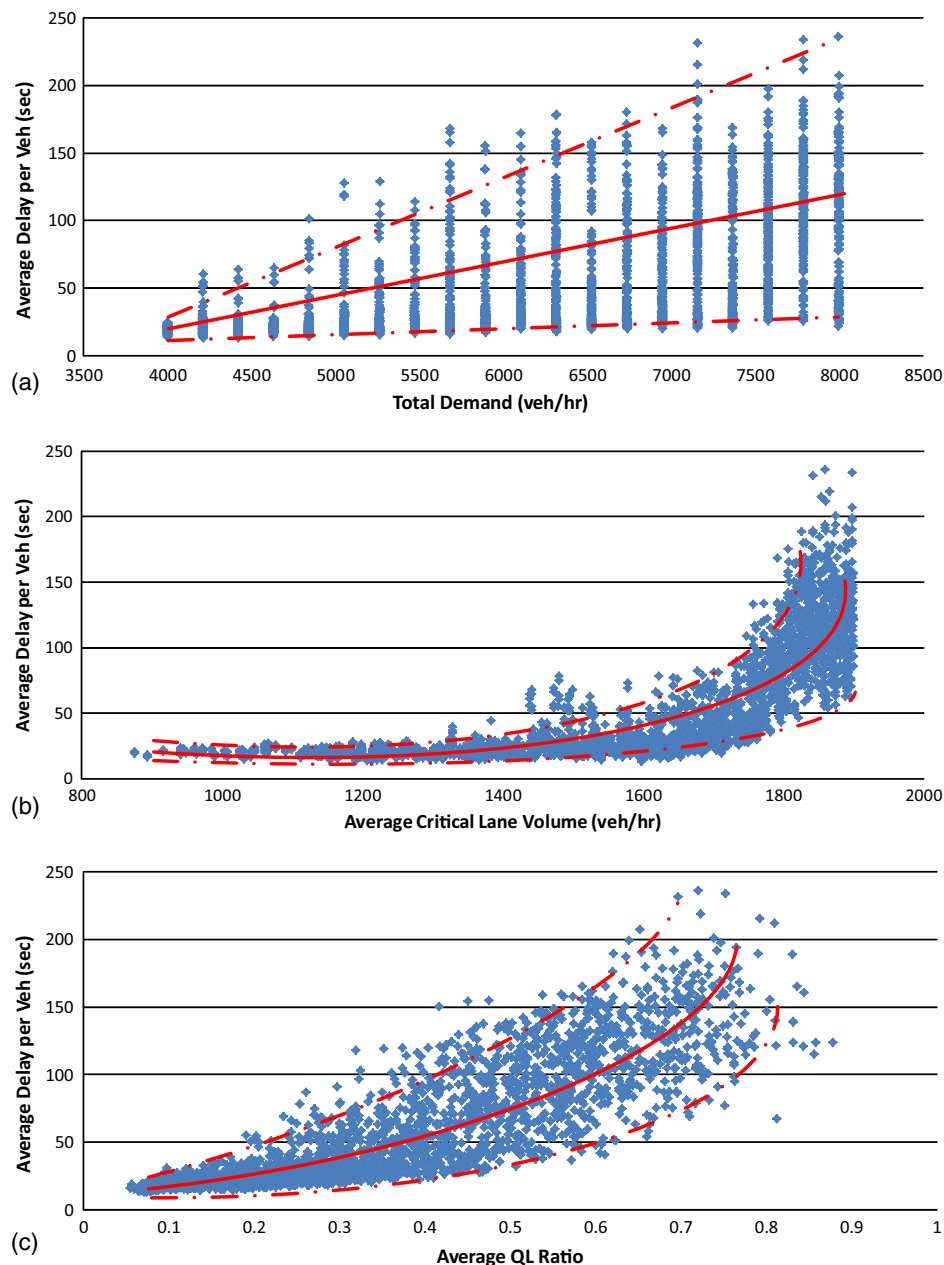| Geometric parameters	A	B	C	D
Left-turn crossover spacing	61 m (200 ft)	91 m (300 ft)	122 m (400 ft)	152 m (500 ft)
Left-turn bay length	76 m (250 ft)	107 m (350 ft)	137 m (450 ft)	168 m (550 ft)
Right-turn bay length	91 m (300 ft)	91 m (300 ft)	91 m (300 ft)	91 m (300 ft)

Fig. 1. Scatter plot of average delay against potential contributing factors

capacity, and the service quality of the entire system may be deteriorated. The average QL ratio is defined as the arithmetic mean of all QL ratios within the CFI design. Similar to the critical lane volume which reflects the saturation level of an intersection, the average QL ratio measures the degree of queue formation with respect to the available bays. Both the mean value and variance of the average delay grow exponentially when the average QL ratio approaches 1. The preceding three experimental results reveal the following critical relationships for our model development:

1. The average delay of CFI depends not only on the total volume, but also the geometric features of the intersection;
2. Compared to the total volume, the CLV of each subintersection is a more reliable indicator to reflect the resulting traffic delay, especially under high congested conditions; and
3. The QL ratio has significant impacts on a CFI's delay. When the average QL ratio of a CFI increases, both the mean and variance of the average delay grows exponentially.

Queue Length Estimation

In view of the high correlation between QL ratios and average intersection delay, this section presents a queue estimation model for each type of bay using a full CFI as an illustrative case. A full-CFI intersection is the most complex and comprehensive design in the CFI family. Fig. 2 shows the classification of all possible queue types based on their geometric features. This study has calibrated the following four equations for those four types of queue at a full-CFI intersection, based on the data generated with the CFI simulator calibrated with field data.

Type-1 Queue (Q_1, Q_5, Q_9, Q_{13})

For those through movements at the major intersection, one can develop a deterministic queue model with the following assumptions: (1) a zero initial queue at the start of green phase,
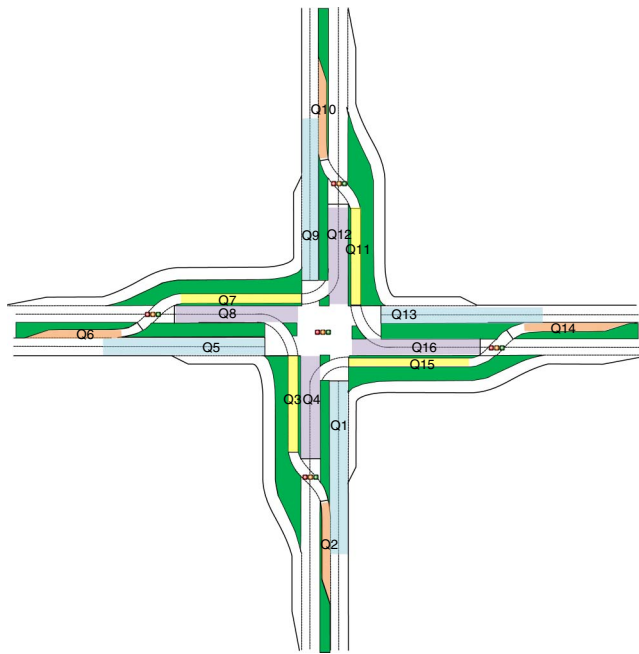
Type-1 Queue (Q_1,Q_5,Q_9,Q_{13}): Through queues at the major intersection;

Type-2 Queue (Q_2,Q_6,Q_{10},Q_{14}): Left-turn queues at the crossover intersection;

Type-3 Queue (Q_3,Q_7,Q_{11},Q_{15}): Left-turn queues at the major intersection;

Type-4 Queue (Q_4,Q_8,Q_{12},Q_{16}): Through queues at the crossover intersection;

Fig. 2. Spatial distributions of potential queue locations at a full-CFI design

(2) a uniform arrival pattern, (3) a uniform departure pattern, (4) arriving volumes do not exceed the intersection capacity.

As shown in Fig. 3, the maximum queue length is obtained at the queue vanish point due to the physical discharging process. Therefore, a simple deterministic queue model is

$$Q = R \cdot q + \frac{R \cdot q}{s - q} \cdot q \qquad (4)$$

where R = red time duration; q = arrival rate; and s = saturation flow rate.

Note that the first component of Eq. (4) is the accumulated queue during the red phase, and the second component is the additional queue due to the discharging shockwave. Eq. (4) could be simplified as

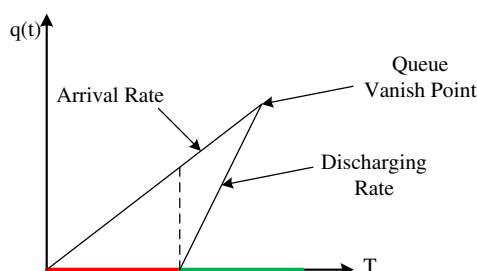$$Q = \frac{R \cdot q \cdot s}{s - q} \qquad (5)$$

Fig. 3. Deterministic queuing process for Type-1 queue

Due to the traffic fluctuation and interdependent relations between neighboring subintersections, the simple deterministic model with Eq. (5) may not fully capture the relation between queue length and its coming volume in a CFI. In addition, the results of extensive simulations experiments indicate that the following factors can significantly impact the formation and dissipation of Type-1 queue: the intersection congested level measured with the critical lane volume (CLV), and QL ratios at the downstream links.

Hence, this study has combined the deterministic component and findings from simulation experiments to develop the following statistical model for estimating the Type-1 queue length (in meters):

$$\underset{t \text{ value}}{\text{Queue}} = \underset{(64.9)}{0.195} \frac{D_t(1 - G_t)s}{s - D_t} + \underset{(126.3)}{1.567} \left(\frac{D_t}{s - CV_m} \right)^2 + \underset{(16.7)}{0.524} e^{\theta \rho_d}$$

$$R^2 = 0.862, \qquad \text{Sample size } N\text{: 2,400}, \qquad t-\text{critical value: 1.96}$$
$$(6)$$

where D_t = approaching through volume (vehicles per hour); G_t = estimated green time ratio for through movements at the major intersection; s = intersection critical lane capacity (i.e., maximum critical lane volume); CV_m = critical lane volume at the major intersection; ρ_d = QL ratio at the downstream link; and θ = model parameter, $\theta = 4$.

Note that the first term in Eq. (6) is based on Eq. (5), and the second term reflects the fact that the queue will grow rapidly if the intersection critical lane volume has reached its capacity.

Type-2 Queue (Q_2, Q_6, Q_{10}, Q_{14})

The formation of a Type-2 queue is due mostly to the left-turn movement and is affected by the potential queue spillback at its downstream location. Using the same methodology for developing the model for Type-1 Queue, the research team has calibrated the following equation for estimating the Type-2 queue length (in meters):

$$\underset{t \text{ value}}{\text{Queue}} = \underset{(234.8)}{0.218} \frac{D_l(1 - G_l)s}{s - D_l} + \underset{(89.3)}{1.914} \left(\frac{D_l}{s - CV_n} \right)^2 + \underset{(8.6)}{0.344} e^{\theta \rho_d}$$

$$R^2 = 0.877, \qquad \text{Sample size } N\text{: 2,400}, \qquad t-\text{critical value: 1.96}$$
$$(7)$$

where D_l = approaching left-turn volume (vehicles per hour); G_l = estimated green time ratio of left-turn movements at the crossover intersection; S = critical lane capacity (i.e., maximum critical lane volume); CV_n = critical lane volume at the crossover intersection; ρ_d = QL ratio at the downstream link; and θ = model parameter, $\theta = 4$.

Type-3 Queue (Q_3, Q_7, Q_{11}, Q_{15})

The formation of a Type-3 queue varies with the green times at two neighboring intersections, as left-turn traffic flows, after crossing the opposing through traffic via the crossover intersection, need to pass the second signal at the primary junction where they can move concurrently with the through (or right-turn) traffic stream.

As shown in Fig. 4, from the start of a green phase at the upstream intersection, the accumulated queuing vehicle shall begin to discharge and travel to the downstream intersection. Some vehicles may pass the downstream intersection without stop due to the signal progression, while some may encounter the red phase and
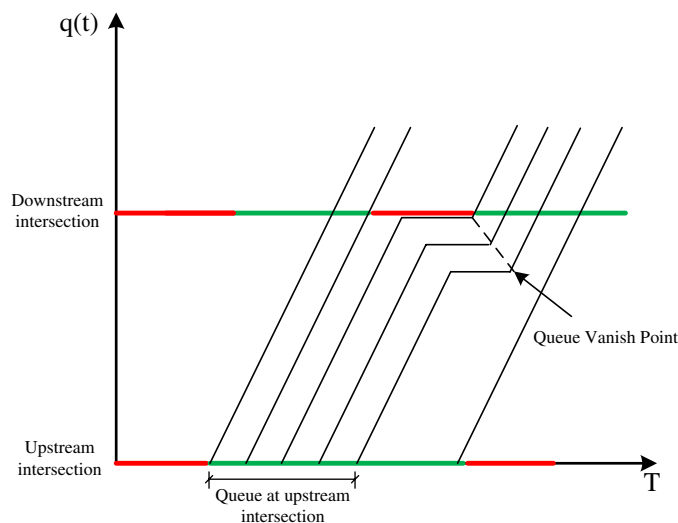
Fig. 4. Deterministic queuing trajectory for Type-3 queue

volume (vehicles per hour); CV_n = critical lane volume at the crossover intersection; G_t = green time ratio for the through movement at the crossover intersection; and S = critical lane capacity (i.e., maximum critical lane volume).

Stability Tests of Queue Models

To further investigate the statistical property of the queue formulas derived from regression, two types of statistical tests have been performed: the Shapiro-Wilk test of normality and the Chow test of model stability. The Shapiro-Wilk test is employed to confirm the estimation error of each queue model follows a normal distribution. As shown in Table 3, all queue models, consistent with the normality test criterion, reflect that the residuals of regression equations follow a normal distribution.

To evaluate the model's stability, the Chow test has also been applied to verify that the coefficients of regression equations do not vary with the sample size. To do so, the original data set of 800 samples has been divided into two subgroups with $n_1 = 600$ and $n_2 = 200$ samples, and the Chow test statistics as follows:

$$F = \frac{[\sum e_p^2 - (\sum e_1^2 + \sum e_2^2)]/K}{(\sum e_1^2 + \sum e_2^2)/(n_1 + n_2 - 2K)} \quad (10)$$

where $\sum e_p^2, \sum e_1^2, \sum e_2^2$ = sum of residual square of the regression model fitted with the original, group 1, and group 2 data sets, respectively; K = number of parameters in regression; and the test results are summarized in Table 4.

The result of stability tests reflects that all estimated model parameters are statistically stable, implying that the estimated queue lengths with the proposed models are statistically reliable for use at the planning stage.

Model Application Process

As discussed previously, the occurrence of blockage at CFI may lead to a significant delay increase, and consequently a reduction of its operational benefits. With the queue estimation models, a planning process is proposed to help engineers in design of a CFI's link length, and to prevent the potential queue spillback.

Demand Pattern and Signal Settings

To apply the proposed queue estimation models, one shall first set the signal timings based on the projected demand level. To reflect the traffic fluctuation over time, a set of demand intervals are defined to represent the upper-bound and lower-bound of the possible

contribute to the queue formation. Also, both the green ratio at downstream intersection and the QL ratio at downstream link can significantly influence the queue length. Hence, one can construct the Type-3 queue model with the following three primary components:

- Impacts due to the queue at the upstream intersection;
- Impact of the downstream red time; and
- Impacts due to the downstream QL ratio.

The calibrated regression model with the preceding key components for the Type-3 queue length (in meters) is given by

$$\underset{t\,\text{value}}{\text{Queue}} = \underset{(17.8)}{0.101} \frac{D_l(1 - G_u)s}{(s - D_l)} + \underset{(15.6)}{0.128} D_l(1 - G_d) + \underset{(7.27)}{0.22} e^{\theta \rho_d}$$

$$R^2 = 0.912, \quad \text{Sample size } N: 2,400, \quad t-\text{critical value: } 1.96 \quad (8)$$

where D_l = approaching left-turn volume (vehicles per hour); G_u = estimated green time ratio of left-turn movements at crossover intersections; G_d = estimated green time ratio of left-turn movements at the major intersection; S = critical lane capacity (i.e., maximum critical lane volume); ρ_d = QL ratio at the downstream link; and θ = model parameter, $\theta = 4$.

Type-4 Queue (Q_4, Q_8, Q_{12}, Q_{16})

Similar to the Type-1 queue, key factors such as the incoming demand to the target approach, the green time ratio, and the intersection congested level measured with the CLV can collectively determine the formation of Type-4 queue. By including all these factors, this study proposes the following model for estimating the Type-4 queue length (in meters):

$$\underset{t\,\text{value}}{\text{Queue}} = \underset{(61.7)}{0.153} \frac{(D_t + D_l)(1 - G_t)s}{s - (D_t + D_l)} + \underset{(56.3)}{0.189} \left(\frac{D_t + D_l}{s - CV_n}\right)^2$$

$$R^2 = 0.817, \quad \text{Sample size } N: 2,400, \quad t-\text{critical value: } 1.96 \quad (9)$$

where D_t = incoming south (north) bound through volume (vehicles per hour); D_l = incoming west (east) bound left-turn

Table 3. Shapiro-Wilk Normality Test Results

Metric	Type-1 queue	Type-2 queue	Type-3 queue	Type-4 queue
W test statistic	0.9855	0.9767	0.9983	0.9972
P-value	1.45×10^{-17}	1.72×10^{-22}	1.63×10^{-3}	1.38×10^{-5}

Table 4. Chow Test Results

Queue model	Test statistic	F value (5%)	Pass?
Type 1	2.37	2.62	Yes
Type 2	2.19	2.62	Yes
Type 3	2.59	2.62	Yes
Type 4	2.93	3.01	Yes

Fig. 5. Signal phase diagram of a full CFI

Fig. 6. Planning-stage flowchart for the design of CFI
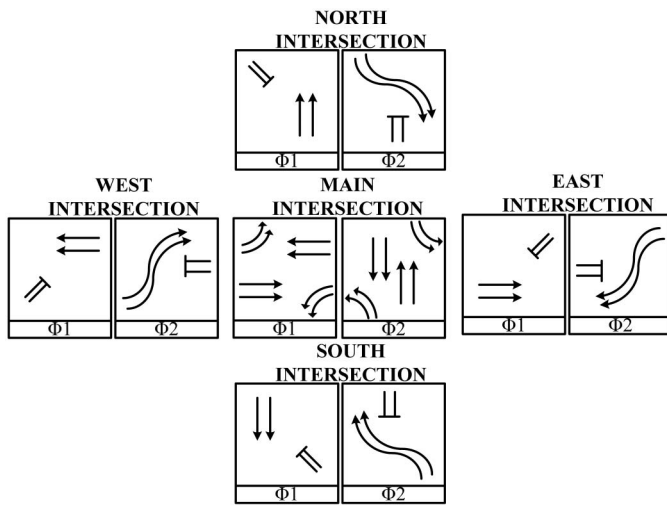
demand patterns. And the actual demand pattern becomes a random value within the given demand intervals.

$$\mathbf{D} = \{\boldsymbol{\lambda}_i; \forall i\} \tag{11}$$

where $\boldsymbol{\lambda}_i$ = demand interval and $\boldsymbol{\lambda}_i = [\underline{\lambda}_i, \overline{\lambda}_i]$.

Due to the unique geometric features of CFIs, the number of conflicted points has been reduced significantly, and a two-phase signal phasing plan is used for both the primary intersection and subintersections. Also, the use of a simple two-phase signal plan is actually one of the primary benefits of the CFI design. A typical simple two-phase signal strategy for CFI is presented in Fig. 5.

Note that the preliminary signal settings at the planning stage are used for queue estimation only. Hence, one can take the following straightforward way to specify signal times based on the projected demand level:

$$\mathbf{g}_i = \frac{\max\{\boldsymbol{\lambda}_i, \boldsymbol{\lambda}_j; j \in V_i\}}{\max\{\boldsymbol{\lambda}_i, \boldsymbol{\lambda}_j; j \in V\} + \max\{\boldsymbol{\lambda}_i, \boldsymbol{\lambda}_j; j \notin V\}} \text{ for each intersection } j \tag{12}$$

where g_i = assigned green ratio of the movement i; λ_i = demand of movement i; and V_i = set of movements that concurrently has the right-of-way with i.

Design Planning and Evaluation Process

As shown in Fig. 2, 16 critical links are identified in a full CFI design, where each link length should be sufficiently long to accommodate the potential traffic queues. With the proposed queue estimation models, the resulting queue length could be estimated as follows:

$$\mathbf{Q}_i = f(\boldsymbol{\lambda}_i, \mathbf{g}_i) = [f(\underline{\lambda}_i, \overline{g}_i), f(\overline{\lambda}_i, \underline{g}_i)] \tag{13}$$

where $f(\cdot)$ indicates the queue estimation model, and interval $\mathbf{Q}_i$ denotes the estimated queue length.

Note that in a real-world application, the actual queue length may be shorter than the estimated result if signals are effectively coordinated. For a conservative design, one can select the length of each CFI's link as follows:

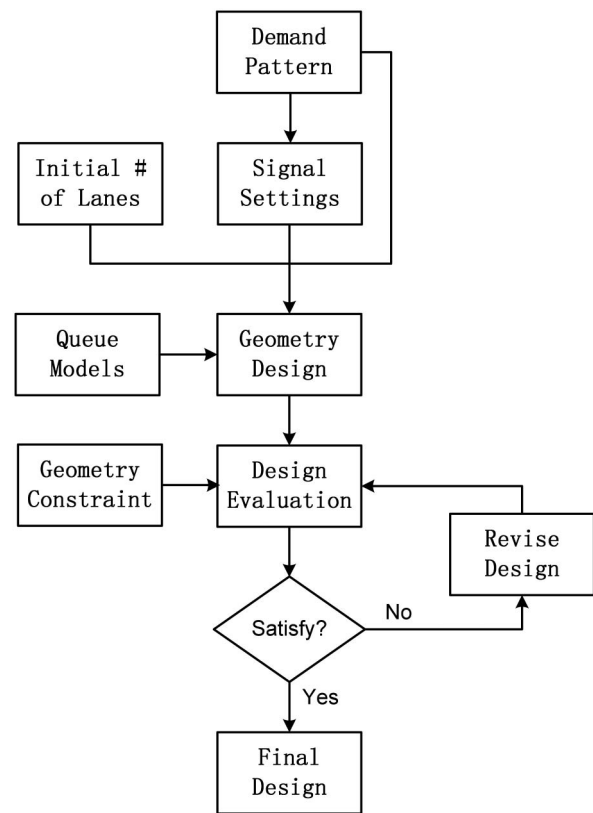$$L_i \geq \underline{Q}_i + \mu(\overline{Q}_i - \underline{Q}_i) \tag{14}$$

where $\overline{Q}_i$ and $\underline{Q}_i$ = upper and lower bound of the queue length; $\mu \in (0, 1)$ and μ is used to select the value between $\overline{Q}_i$ and $\underline{Q}_i$ so as to prevent a conservative design. Based on experimental experience, the suggested value range is 0.6–0.9.

Also note that the available right-of-way may limit the design of a link length. For instance, the distance to adjacent intersections will limit the length of a CFI's leg. Alternatively, one could increase the number of lanes for the particular link when the potential traffic queue exceeds its upper bound.

Fig. 6 illustrates the entire process for CFI planning and evaluation, based on all the preceding steps.

Case Study

To evaluate the proposed planning model, a real-world case study is presented in this section. Fig. 7 shows the current design at the intersection of MD 4 and MD 235 and the layout of the proposed CFI design.

The proposed full CFI is designed to contend with the heavy and unbalanced traffic volumes during the peak hours. The morning and afternoon peak hour traffic demands to this site were collected from field surveys and are shown in Table 5.

Some key parameters are initially set as follows:
- The maximum link length for the crossover space is 122 m (400 ft);
- The maximum link length for the left-turn bay is 135 m (450 ft);
- Leg 1: 2 lanes for left-turn link, 3 lanes for through link and 1 lane for right-turn link;
- Leg 2: 1 lanes for left-turn link, 1 lanes for through link and 1 lane for right-turn link;
- Leg 3: 1 lanes for left-turn link, 3 lanes for through link and 1 lane for right-turn link;
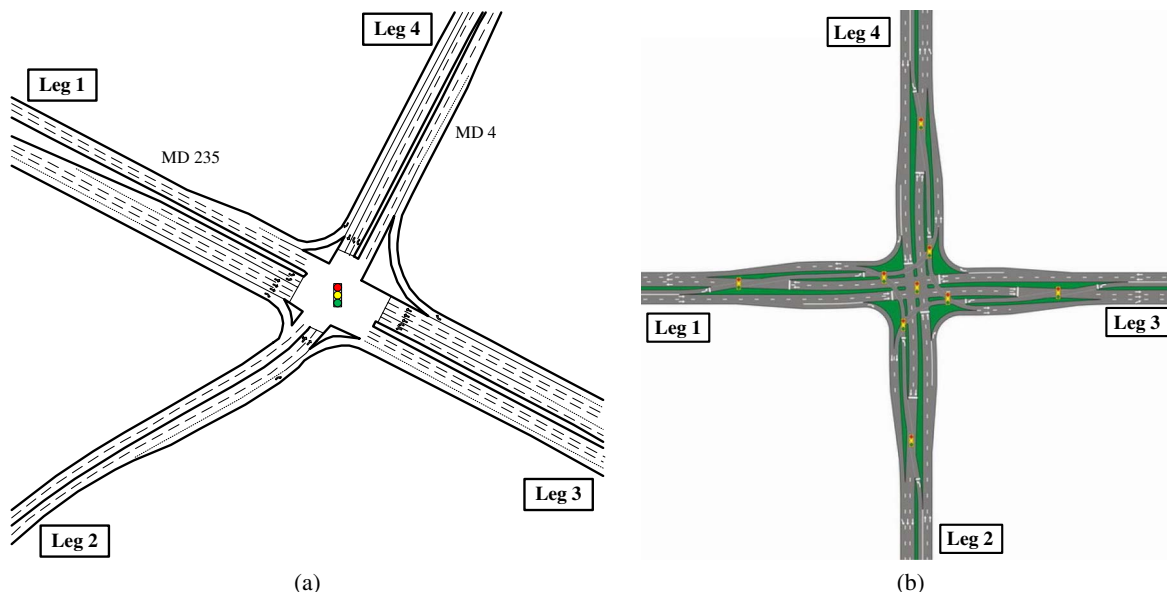
Fig. 7. Geometry design of intersection MD 4 at MD 235: (a) overhead view of the current intersection; (b) proposed continuous-flow intersection

Table 5. Morning and Afternoon Peak Hour Demand and Demand Interval

Direction	Left-turn (veh/h)		Through (veh/h)		Right-turn (veh/h)	
	a.m./p.m.	Interval	a.m./p.m.	Interval	a.m./p.m.	Interval
Eastbound	250/575	[250, 575]	2,475/1,675	[1,675, 2475]	75/125	[75, 125]
Northbound	100/125	[100, 125]	250/425	[250, 425]	350/200	[200, 350]
Westbound	175/400	[175, 400]	1,150/2,325	[1,150, 2,325]	475/1,375	[475, 1,375]
Southbound	1,700/825	[825, 1,700]	325/400	[325, 400]	450/375	[375, 450]

- Leg 4: 2 lanes for left-turn link, 1 lanes for through link and 1 lane for right-turn link; and
- The constant parameter μ is assumed to be 0.7.

Following the proposed planning procedure, the authors first estimate the potential queue length for each turning and through traffic flows and then determine the link length based on the estimation results. To facilitate the presentation, let L1 be denoted as the left-turn bay (Q2, Q6, Q10, Q14 in Fig. 2); L2 as the left-turn crossover link (Q3, Q7, Q11, Q15 in Fig. 2); T1 as the through crossover link (Q4, Q8, Q12, Q16 in Fig. 2); and T2 as the through link (Q1, Q5, Q9, Q13 in Fig. 2). The initial designs of signal settings are listed in Table 6.

As shown in Table 6, some computed link lengths (i.e., T1, L2 and T2 at Leg 3) exceed the maximum link length constraint. The violation of constraints at Leg 3 is because of the long queue (191 m) at T1. Obviously, a direct thinking is to increase the number of lanes at T1. However, three lanes are already selected in the current design plan, and increasing the number of lane at that location may not be a good option. Note that traffic queue is directly impacted by the arrival rate and signal timings. Hence, an alternative way is to increase the number of lanes at its opposite location (L1 of Leg 3). Consequently, the green ratio of movement at T1 could be increased due to the reduced green ratio of movement at L1. The final design plan is shown in the Table 7.

With the revised geometry parameter, *VISSIM* was used as the unbiased platform to evaluate the proposed CFI and the current conventional intersection. Table 8 summarizes the performance comparison between these two designs, using a 1-h simulation.

Table 8 shows a significant reduction in both the total travel time and average delay with the CFI design. There are two plausible

Table 6. Initial Design of CFI

Location		Number of lanes	Estimated queue (m)	Required link length (m)	Designed link length (m)	Max link length (m)	Satisfy
Leg 1	L1	2	[22, 57]	46	61	122	Yes
	T1	3	[22, 61]	49	76	137	Yes
	L2	2	[18, 44]	36	76	137	Yes
	T2	3	[81, 156]	134	137	259	Yes
Leg 2	L1	1	[20, 25]	23	46	122	Yes
	T1	1	[16, 34]	29	46	137	Yes
	L2	1	[16, 20]	19	46	137	Yes
	T2	1	[31, 60]	51	92	259	Yes
Leg 3	L1	1	[34, 91]	74	76	122	Yes
	T1	3	[65, 246]	**191**	**198**	**137**	**No**
	L2	1	[26, 66]	**54**	**198**	**137**	**No**
	T2	3	[48, 139]	**112**	**274**	**259**	**No**
Leg 4	L1	2	[45, 141]	112	116	122	Yes
	T1	2	[28, 68]	56	107	137	Yes
	L2	2	[48, 121]	99	107	137	Yes
	T2	1	[42, 55]	51	223	259	Yes

Note: The length of T2 is the sum of L1 length and L2 (or T1) length; the length of T1 is equal to L2 length; the number of lanes at downstream link should be larger or equal to the one at upstream link. Bold font indicates computed link lengths that exceed the maximum link length constraint.

reasons for having such improvements. First, the proposed CFI design eliminates the left-turn flows from the through volume, which consequently reduces the number of signal phases and improves the level of service at the center intersection. Secondly, the CFI has a

1130 / JOURNAL OF TRANSPORTATION ENGINEERING © ASCE / NOVEMBER 2013

Table 7. Final Design of CFI

Location		Number of lanes	Estimated queue (m)	Required link length (m)	Designed link length (m)	Max link length (m)	Satisfy
Leg 1	L1	2	[22, 57]	46	61	122	Yes
	T1	3	[22, 61]	49	76	137	Yes
	L2	2	[18, 44]	36	76	137	Yes
	T2	3	[81, 156]	134	137	259	Yes
Leg 2	L1	1	[20, 25]	23	46	122	Yes
	T1	1	[16, 34]	29	46	137	Yes
	L2	1	[16, 20]	19	46	137	Yes
	T2	1	[31, 60]	51	92	259	Yes
Leg 3	L1	2	[18, 44]	36	46	122	Yes
	T1	3	[35, 137]	106	107	137	Yes
	L2	2	[14, 33]	27	107	137	Yes
	T2	3	[46, 139]	112	153	259	Yes
Leg 4	L1	2	[45, 141]	112	116	122	Yes
	T1	2	[28, 68]	56	107	137	Yes
	L2	2	[48, 121]	99	107	137	Yes
	T2	1	[42, 55]	51	223	259	Yes

larger geometry layout to prevent the occurrence of queue spillbacks. However, the reduction of average number of stops is not quite significant, due to the increased number of intersections. The measure of effectiveness (MOEs) improvement of CFI clearly shows the potential effectiveness of the proposed planning models.

To further evaluate the revised CFI design in Table 7, the authors have randomly generated 70 demand patterns within the input demand intervals. Because a proper design shall offer sufficient link length to store the potential traffic queue, the defined QL ratio is selected as the direct indicator of lane blockage. Fig. 8 presents the average and maximum QL ratio over 70 scenarios at each critical location.

Obviously, one can observe that all designed links are sufficient to accommodate the traffic queue for most cases (the mean QL ratios are all less than 1.0), revealing the effectiveness of the proposed planning process. Also note that the max QL ratio exceeds 1.0 at Leg 1-T1 and Leg 4-L2, which indicates the potential occurrence of blockage at the worst scenario. However, to prevent an overconservative design, such results are viewed as acceptable in practice in view of the construction cost with a larger footprint. Because the QL ratio is small at other links, an alternative way to prevent those potential blockages is to increase the green time for those congested movements.
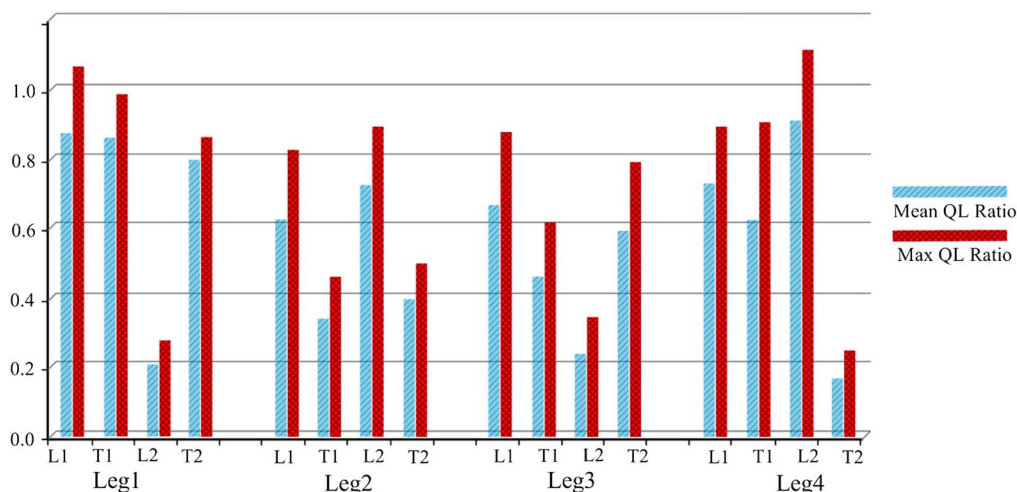
Conclusions

This paper has proposed a planning process and models for a CFI's geometry design. Due to the interdependent nature of traffic queues among the five closely spaced intersections of a CFI, the proposed process includes the QL ratio as its key variable, offering an effective and convenient way for users to identify any potential queue spillback location. Based on the experimental data, this study has further conducted a comprehensive analysis of CFI with respect to the total delay, and confirmed the intercorrelation between delay and QL ratio at each critical location. The set of queue estimation models developed in this study offers an effective tool for highway designers to compute proper link lengths for both through and left-turn movements in CFI. Recognizing the limit of available real-world data, this study has employed microscopic simulation results for model development. Compared with the conventional intersection, the proposed CFI design was able to significantly reduce the total travel time and average delay per vehicle for the studied cases.

Research is ongoing to further investigate the complex interrelations between the queue formation and dissipation among a CFI's

Table 8. Performance Comparisons between Different Scenarios

Time	Design	Average delay per vehicle (s)	Improvement	Total travel time (h)	Improvement	Average number of stops per vehicle	Improvement
Morning peak	Conventional	92.727	—	216.039	—	2.041	—
	CFI design	61.058	−34.2%	183.461	−15.1%	1.913	−6.3%
Afternoon peak	Conventional	86.278	—	201.825	—	2.194	—
	CFI design	56.021	−35.1%	172.227	−14.7%	2.023	−7.8%

Fig. 8. Evaluated QL ratios over 70 scenarios (mean and max)

five intersections under various signal control plans. The results of delay and queue analyses at the operational level can also serve as the basis for development of signal optimization model for CFI.

Acknowledgments

References

Cheong, S., Rahwanji, S., and Chang, G. L. (2008). "Comparison of three unconventional arterial intersection designs: continuous flow intersection, parallel flow intersection, and upstream signalized crossover." *11th Int. IEEE Conf.* New York.

El Esawey, M., and Sayed, T. (2007). "Comparison of two unconventional intersection schemes." *Transportation Research Record No. 2023*, Transportation Research Board, Washington, DC, 10–19.

Goldblatt, R., Mier, F., and Friedman, J. (1994). "Continuous flow intersection." *J. Inst. Transport. Eng.*, 64(7), 34–42.

Hildebrand, T. E. (2007). "Unconventional intersection designs for improving through traffic along the arterial road." Ph.D. Thesis, Dept. of Civil and Environmental Engineering, Florida State Univ., Tallahassee, FL.

Hughes, W., Jagannathan, R., Sengupta, D., and Hummer, J. (2010). "Alternative intersections/interchanges: Information report (AIIR)." *FHWA-HRT-09-060*, Federal Highway Administration, Washington, DC, 7–70.

Hummer, J. E. (1998a). "Unconventional left-turn alternative for urban and suburban arterials: Part One." *ITE Journal*, 68(9), 26–29.

Hummer, J. E. (1998b). "Unconventional left-turn alternative for urban and suburban arterials: Part Two." *ITE J. Web*, 101–106.

Inman, V. W. (2009). "Evaluation of signs and markings for partial continuous flow intersectionS." *Transportation Research Record 2138*, Transportation Research Board, Washington, DC, 66–74.

Jagannathan, R., and Bared, J. G. (2004). "Design and operational performance of crossover displaced left-turn intersections." *Transportation Research Record 1981*, Transportation Research Board, Washington, DC, 86–96.

Kim, M., Lai, X., Chang, G. L., and Rahwanji, S. (2007). "Unconventional arterial designs initiatives." *IEEE Conf. on Intelligent Transportation Systems*, Seattle.

Pitaksringkarn, J. P. (2005). "Measures of effectiveness for continuous flow intersection: A Maryland intersection case study." *ITE 2005 Annual Meeting and Exhibit Compendium of Technical Papers*, Institute of Transportation Engineers, ARRB Group, Australia.

Reid, J. D., and Hummer, J. E. (1999). "Analyzing system travel time in arterial corridors with unconventional designs using microscopic simulation." *Transportation Research Record 1678*, Transportation Research Board, Washington, DC, 208–215.

Reid, J. D., and Hummer, J. E. (2001). "Travel time comparisons between seven unconventional arterial intersection designs." *Transportation Research Record 1751*, Transportation Research Board, Washington, DC, 55–56.